

Primitive-Driven Acceleration of Hyperdimensional Computing for Real-Time Image Classification

Dhruv Parikh, Jebacyril Arockiaraj, and Viktor Prasanna

University of Southern California, Los Angeles, CA, USA

{dhruvash, arockiar, prasanna}@usc.edu

Abstract—Hyperdimensional Computing (HDC) represents data using extremely high-dimensional, low-precision vectors—termed hypervectors (HVs)—and performs learning and inference through lightweight, noise-tolerant operations. However, the high dimensionality, sparsity, and repeated data movement involved in HDC make these computations difficult to accelerate efficiently on conventional processors. As a result, executing core HDC operations—binding, permutation, bundling, and similarity search—on CPUs or GPUs often leads to suboptimal utilization, memory bottlenecks, and limits on real-time performance.

In this paper, our contributions are two-fold. First, we develop an image-encoding algorithm that, similar in spirit to convolutional neural networks, maps local image patches to hypervectors enriched with spatial information. These patch-level hypervectors are then merged into a global representation using the fundamental HDC operations, enabling spatially sensitive and robust image encoding. This encoder achieves 95.67% accuracy on MNIST and 85.14% on Fashion-MNIST, outperforming prior HDC-based image encoders. Second, we design an end-to-end accelerator that implements these compute operations on an FPGA through a pipelined architecture that exploits parallelism both across the hypervector dimensionality and across the set of image patches. Our Alveo U280 implementation delivers 0.09 ms inference latency, achieving up to 1300 \times and 60 \times speedup over state-of-the-art CPU and GPU baselines, respectively.

Index Terms—Hyperdimensional Computing, Hypervectors, FPGA Acceleration, Image Classification, Real-Time Systems, Patch-Based Encoding, Parallel Processing, Low-Power Computing.

I. INTRODUCTION

Hyperdimensional Computing (HDC) represents data using high-dimensional, low-precision hypervectors and manipulates them with a small set of algebraic primitives such as bundling, binding, and permutation [1]–[4]. These operations enable robust, noise-tolerant learning and lend themselves naturally to bit-level and word-level parallelism, making HDC attractive for edge and resource-constrained platforms [5]. HDC has been successfully applied to biosignals, speech, DNA analytics, and human activity recognition [6]–[11], often achieving competitive accuracy with significantly lower computational cost.

Recent work has focused on improving hypervector design and encoding strategies to bridge the accuracy gap with deep learning while preserving HDC’s efficiency. This includes hardware-aware hypervector construction [12], encoding for binarized images [13], static optimization of HDC computations [14], and ultra-efficient engines tailored to IoT workloads [15]. In parallel, trainable and adaptive encoders [16]–

[18] and algorithm–hardware co-design techniques [19] have demonstrated that modest learning capacity and task-aware encodings can substantially improve classification accuracy without abandoning HDC’s lightweight primitives.

However, image-specific HDC methods remain comparatively underexplored. Existing work on image classification with HDC often treats images as unordered collections of pixels or handcrafted descriptors, or emphasizes privacy and energy efficiency rather than spatially structured representations [13], [20]–[22]. These approaches typically lack an explicit notion of patch-level receptive fields and spatial permutation analogous to convolutional neural networks, and they seldom study how such encoders map to concrete hardware implementations for real-time deployment. As a result, there is a gap between the algorithmic potential of HDC for image data and its realization as a low-latency, hardware-efficient pipeline.

On the hardware side, a growing body of work accelerates generic HDC workloads on CPUs, GPUs, FPGAs, and processing-in-memory (PIM) substrates [5], [23]–[27]. CPU and GPU frameworks exploit wide SIMD units and multi-core parallelism, but they are typically optimized for large batches and struggle to deliver ultra-low latency when processing a continuous stream of small images in real time. FPGAs, in contrast, can implement custom, streaming dataflow architectures that fuse binding, bundling, permutation, and similarity search into deeply pipelined engines with fine-grained control over memory bandwidth and on-chip parallelism [26]. Yet prior FPGA designs generally target 1D or tabular workloads and do not co-design the HDC encoder and hardware around image patches and hypervector structure.

In this work, we bridge these gaps by co-designing a patch-based HDC image encoder and a primitive-driven FPGA accelerator for real-time image classification. Our key contributions are:

- We propose a spatially aware, patch-based HDC encoder that maps local image regions to hypervectors using position- and intensity-dependent banks, aggregates them via permutation and bundling, and refines class hypervectors using similarity-guided online updates. This design achieves higher accuracy than prior HDC image encoders on MNIST and Fashion-MNIST while preserving simple, composable primitives.
- We design an end-to-end FPGA accelerator that realizes the complete HDC inference pipeline—patch encoding,

global accumulation, and similarity search—as a streaming dataflow architecture. The accelerator exploits parallelism both along the hypervector dimension and across image patches using a patch processor array, a global adder tree, and a similarity engine mapped to an Alveo U280 FPGA.

- We provide a comprehensive evaluation across CPU, GPU, and FPGA platforms, showing that our FPGA design delivers orders-of-magnitude lower single-image latency and higher throughput than optimized PyTorch baselines, while maintaining competitive accuracy. Ablation studies on patch size and hypervector dimension further quantify the trade-offs between accuracy and hardware efficiency.

II. RELATED WORK

HDC fundamentals and learning frameworks. Hyperdimensional Computing (HDC) has been widely studied as a robust, compact alternative to conventional machine learning, grounded in high-dimensional random representations and simple algebraic primitives [1]–[3]. A variety of methods improve HDC’s encoding and learning capabilities through quantization [28], stochastic and memory-centric training [29], federated or dynamic updates [30], [31], and trainable encoders [16], [17]. Recent work such as LaplaceHDC [32] refines the geometric interpretation of binary hypervectors, while LeHDC [33] introduces learning-based prototype construction for improved accuracy. These methods demonstrate that modest learning capacity can substantially enhance HDC performance while retaining lightweight, interpretable operations.

HDC for image classification. Although numerous HDC encoders exist for biosignals, text, and tabular data [6], [7], [10], image-specific HDC remains comparatively limited. Prior work has proposed binarized or static image encodings [13], descriptor aggregation frameworks [21], and privacy-preserving image representations [22], but these approaches typically lack explicit spatial structure, patch semantics, or principled permutation-based aggregation. More advanced methods such as ManiHD [18] and QuantHD [28] introduce trainable or quantized pipelines but do not target spatially coherent image encoding comparable to convolutional receptive fields.

Hardware acceleration of HDC. HDC has been accelerated on CPUs, GPUs, FPGAs, and PIM architectures using vectorization, parallel training, or custom logic [23]–[27]. GPU-centric designs typically rely on large batches to exploit data parallelism via SIMD, while FPGA implementations leverage dataflow pipelines for low-latency streaming inference. Existing FPGA accelerators, however, primarily target 1D or tabular HDC workloads rather than spatially structured image encoders [29]–[33]. Our work differs by co-designing a patch-based HDC algorithm with an FPGA-friendly architecture, enabling fine-grained patch-level and hypervector-level parallelism tailored for real-time image classification.

III. PRELIMINARIES

A. Hyperdimensional Computing

Hyperdimensional Computing (HDC) represents data using high-dimensional *hypervectors* (HVs) of dimension D , typically $D \sim 10^3\text{--}10^5$. We use bipolar HVs $\mathbf{h} \in \{-1, +1\}^D$, which enable simple, highly parallel element-wise operations. HDC relies on three fundamental primitives:

- **Bundling** (\oplus): element-wise addition followed by bipolarization, $\mathbf{h} = \text{sign}(\mathbf{h}_1 + \mathbf{h}_2 + \dots)$, producing an HV similar to its constituents.
- **Binding** (\odot): element-wise multiplication, $\mathbf{h} = \mathbf{h}_1 \odot \mathbf{h}_2$, generating an HV dissimilar to both inputs and used to associate features with positions or symbols.
- **Permutation** (π): cyclic rotation, $\pi^t(\mathbf{h})$, used to encode structural, temporal, or positional information such as a sequence index or patch ID.

These operations map raw features into high-dimensional representations that can be compared efficiently using cosine or Hamming similarity. High dimensionality provides inherent robustness: perturbing a small fraction of dimensions rarely alters similarity relationships between HVs.

B. HDC Classification Model

In a standard HDC classifier, each class c is represented by a prototype hypervector $\mathbf{C}_c \in \{-1, +1\}^D$. During training, prototypes are formed by bundling the encoded HVs of all samples with label c : $\mathbf{C}_c \leftarrow \text{sign}(\sum_{n:y^{(n)}=c} \mathbf{H}^{(n)})$. At inference time, an input is encoded into a query HV \mathbf{H} using a task-specific encoder built from binding, bundling, and permutation. Classification is performed via nearest-prototype matching: $\hat{y} = \arg \max_c \text{sim}(\mathbf{H}, \mathbf{C}_c)$, where $\text{sim}(\cdot, \cdot)$ denotes cosine similarity or Hamming distance.

IV. METHOD

We now describe our primitive-driven HDC algorithm and accelerator for real-time image classification. Section IV-A presents the patch-based image encoder and online hypervector learning procedure [34], while Section IV-B details the FPGA accelerator architecture that implements this algorithm as a deeply pipelined dataflow engine.

A. Image Encoding and Online Hypervector Learning

Our approach maps each input image $\mathbf{X} \in \mathbb{R}^{H \times W}$ into a single bipolar hypervector $\mathbf{H} \in \{-1, +1\}^D$, which is then used for incremental hypervector-based learning. The method consists of three stages: pixel-level encoding, patch aggregation with spatial permutation, and global bundling followed by online learning.

Hypervector Banks. We initialize two banks of real-valued hypervectors: a base bank $\mathbf{B}_{i,j} \in \mathbb{R}^D$ for each pixel position (i, j) and a level bank $\mathbf{L}_\ell \in \mathbb{R}^D$ for each quantized intensity level $\ell \in \{0, \dots, L-1\}$. All hypervectors are sampled i.i.d. from a Gaussian distribution and ℓ_2 -normalized along their dimensional axis, $\mathbf{B}_{i,j} \leftarrow \mathbf{B}_{i,j} / \|\mathbf{B}_{i,j}\|_2$ and $\mathbf{L}_\ell \leftarrow \mathbf{L}_\ell / \|\mathbf{L}_\ell\|_2$.

Pixel Encoding. Each pixel value $x_{i,j}$ is first linearly quantized using a scale-zero-point transformation. Let s and z

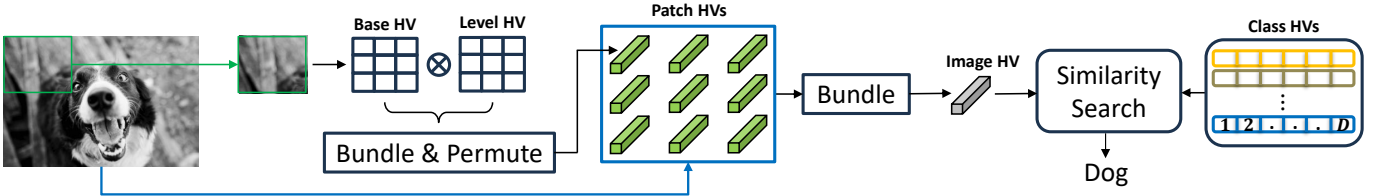


Fig. 1. Overall patch-based HDC encoding pipeline (during inference).

denote the quantization scale and zero-point that map the input range of an image to the integer interval $[0, 255]$. The quantized level is

$$\ell_{i,j} = \text{clip}\left(\left\lfloor \frac{x_{i,j}}{s} + z \right\rfloor, 0, L-1\right), \quad L = 256.$$

A pixel hypervector is then formed by binding the corresponding base and level hypervectors:

$$\mathbf{p}_{i,j} = \mathbf{B}_{i,j} \odot \mathbf{L}_{\ell_{i,j}}.$$

Patch Aggregation. We extract local image regions using square patches of size $M \times M$, analogous to a convolutional kernel of size M . The patch window is moved across the image with a chosen stride r , producing a grid of $K_H \times K_W$ patches. Let \mathcal{P}_t denote the set of pixel coordinates in the t -th patch, where $t \in \{0, \dots, K_H K_W - 1\}$. For each patch, we sum its pixel hypervectors,

$$\tilde{\mathbf{h}}_t = \sum_{(i,j) \in \mathcal{P}_t} \mathbf{p}_{i,j},$$

and apply a permutation (cyclic rotation) indexed by the patch ID t ,

$$\mathbf{h}_t = \pi^t(\tilde{\mathbf{h}}_t), \quad [\pi^t(\tilde{\mathbf{h}}_t)]_d = \tilde{h}_{t, (d-t) \bmod D}.$$

Global Image HV. Patch hypervectors are bundled by summation $\tilde{\mathbf{H}} = \sum_t \mathbf{h}_t$. The final image representation is obtained via bipolar binarization, $H_d = +1$ if $\tilde{H}_d \geq 0$ and $H_d = -1$ otherwise, resulting in $\mathbf{H} \in \{-1, +1\}^D$.

Similarity & Prediction. For each class $c \in \{1, \dots, C\}$ we maintain a class hypervector $\mathbf{C}_c \in \{-1, +1\}^D$ obtained by bundling the image hypervectors belonging to that class. During training, each encoded sample \mathbf{H} is added to the corresponding class sum, and the final class hypervectors are obtained by applying a bipolarization step,

$$\mathbf{C}_c \leftarrow \text{sign}\left(\sum_{\mathbf{H} \in \mathcal{D}_c} \mathbf{H}\right), \quad c = 1, \dots, C.$$

Given an encoded image hypervector \mathbf{H} , we classify it by computing its cosine similarity to each class hypervector,

$$s_c = \frac{\mathbf{H}^\top \mathbf{C}_c}{D}, \quad s_c \in [-1, +1],$$

where division by D normalizes the bipolar inner product and makes the score equivalent to cosine similarity for $\{-1, +1\}$ hypervectors. We get the final predicted label via $\hat{y} = \arg \max_c s_c$.

Online Learning. To refine the class hypervectors beyond the initial bundled prototypes, we use a similarity-weighted corrective update applied only to misclassified samples. Let $s_c \in [-1, +1]$ denote the cosine similarity between an image hypervector \mathbf{H} and class hypervector \mathbf{C}_c , as defined above. For update purposes, this score is shifted to the interval $[0, 1]$ via $\sigma_c = \frac{s_c+1}{2}$. After the initial single-pass construction of the class hypervectors, we run a few retraining epochs in which each misclassified sample with true label y and predicted label \hat{y} triggers the updates

$$\mathbf{C}_y \leftarrow \mathbf{C}_y + \eta(1 - \sigma_y)\mathbf{H}, \quad \mathbf{C}_{\hat{y}} \leftarrow \mathbf{C}_{\hat{y}} - \eta(1 - \sigma_{\hat{y}})\mathbf{H},$$

where η is a learning rate. After retraining, the class hypervectors are binarized using $\text{sign}(\cdot)$ and the resulting bipolar vectors are used for inference.

Overall Algorithm. Algorithm 1 summarizes the full pipeline, with the inference procedure visualized in Fig. 1.

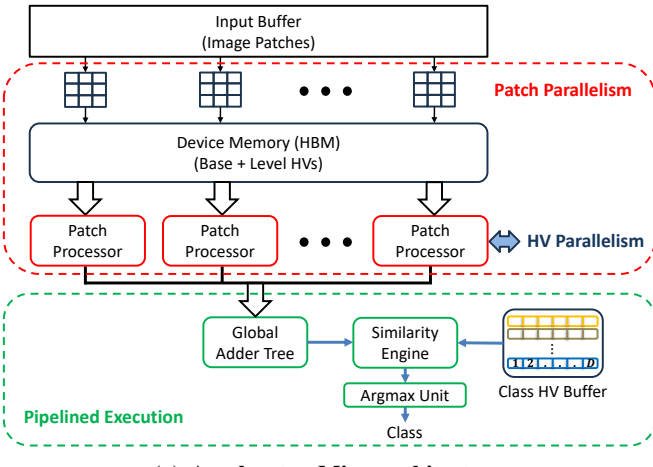
B. Accelerator Architecture

Our accelerator implements the complete patch-based HDC inference as a deeply pipelined dataflow architecture composed of four compute engines: a patch processor array, a global adder tree, a similarity engine, and a lightweight argmax unit. Parallelism is exploited across both the hypervector dimensionality and the total number of image patches.

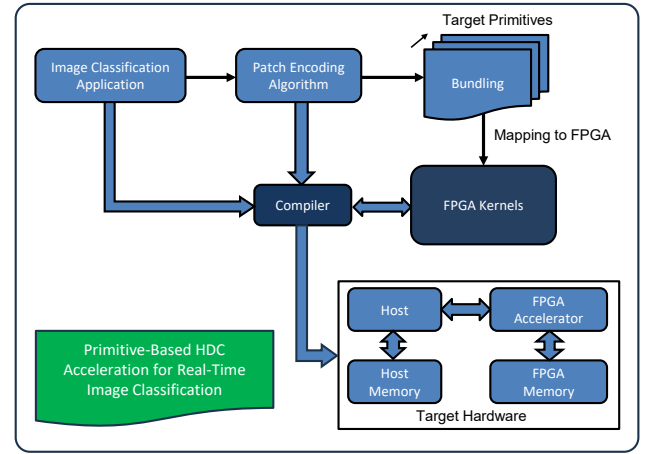
Patch Processor Array. The accelerator instantiates P_{patch} parallel patch processors, each responsible for encoding one $M \times M$ image patch. A patch processor contains P_D parallel vector (MAC) lanes that operate across the hypervector dimension. For each patch, the processor streams in the M^2 base and level hypervectors, performs element-wise binding using the P_D lanes, and accumulates the results into a local P_D -wide buffer. After processing all M^2 pixels, the processor applies the patch-dependent permutation via a barrel-shifter and emits a partial patch hypervector of length P_D . This engine forms the backbone of the accelerator, enabling parallelism both across patches and across hypervector dimensions.

Global Adder Tree. Patch hypervectors produced by the processor array are streamed into a global adder tree. The tree reduces the P_{patch} incoming patch outputs into a single partial image hypervector corresponding to the current P_D -wide segment of the global D -dimensional representation. The adder tree is fully pipelined and processes one set of patch results per cycle.

Similarity Engine. The similarity engine computes dot-product similarity between each incoming hypervector seg-



(a) Accelerator Microarchitecture



(b) Mapping to FPGA Kernels

Fig. 2. Overview of the proposed primitive-driven HDC acceleration framework. (a) The accelerator architecture exposes both patch-level and hypervector-level parallelism using multiple patch processors, a global adder tree, a similarity engine, and a lightweight argmax unit. (b) End-to-end system mapping from the patch-based encoding algorithm to FPGA compute kernels and host-device execution flow.

ment and all class hypervectors. It consists of a bank of P_D parallel multiply-accumulate (MAC) units that process one P_D -dimensional segment at a time. For each segment, the engine multiplies the P_D elements of the image hypervector with the corresponding P_D elements of every class hypervector, accumulating the partial products into a score buffer whose size equals the number of classes. As successive segments are streamed in, the accumulated scores are updated. After all $\lceil D/P_D \rceil$ segments have been processed, the score buffer contains the complete similarity values for all classes.

Argmax Unit. Once all hypervector segments have been processed, the accumulated similarity scores for all classes are streamed into a compact argmax unit. This unit identifies the predicted class label using a pipelined comparator tree.

End-to-End Streaming Dataflow. The accelerator operates as a multi-stage streaming pipeline (Fig. 2). Base and level hypervectors are fetched from on-device memory and delivered to the P_{patch} patch processors, each of which encodes its assigned $M \times M$ patch using P_D concurrent MAC operations per cycle per patch processor. As soon as a partial patch hypervector segment is generated, it is forwarded to the global adder tree, which progressively accumulates contributions from all patches to form the corresponding segment of the image hypervector. The similarity engine consumes each segment immediately, performing dot-product similarity against all class hypervectors and updating a running similarity buffer. After all hypervector segments have been processed, the accumulated scores are passed to a lightweight argmax unit to determine the final predicted class. This design exposes two complementary forms of parallelism: (i) *hypervector parallelism* via P_D concurrent MAC operations per cycle per patch processor, and (ii) *patch-level parallelism* via P_{patch} independent patch processors. Together, these dimensions enable a fully pipelined, low-latency realization of the HDC inference pipeline in Algorithm 1.

TABLE I
SUMMARY OF DATASETS USED IN EVALUATION.

Dataset	Image Size	# Classes	Train / Test
MNIST	28×28	10	60K / 10K
Fashion-MNIST	28×28	10	60K / 10K

TABLE II
HARDWARE PLATFORMS USED IN OUR EVALUATION.

Platforms	CPU	GPU	FPGA
Device	EPYC 7313 (2x)	RTX 6000 Ada	Alveo U280
Process Node	TSMC 7 nm	TSMC 4N (4 nm)	TSMC 16 nm
Compute Units	32C/64T	18,176 CUDA cores	9024 DSP slices
Memory	DDR4 (Host)	48 GB GDDR6	8 GB HBM2
Bandwidth	205 GB/s	960 GB/s	460 GB/s
Frequency	3.7 GHz	2.5 GHz (boost)	300–600 MHz
Peak FP32	–	91.1 TFLOPS	–

V. EXPERIMENTS

A. Datasets

We evaluate our method on two standard image-classification benchmarks: MNIST [35] and Fashion-MNIST [36]. Both datasets consist of 28×28 grayscale images across 10 classes. Following common practice in HDC-based image encoding, all images are zero-padded to 32×32 before patch extraction and quantized to $[0, 255]$ using an affine scale-zero-point mapping.

B. Implementation Setup

Hardware Platforms. We evaluate our approach on three representative platforms summarized in Table II. For the CPU baseline, we use a dual-socket AMD EPYC 7313 server with 32 cores / 64 threads and DDR4 host memory. The GPU baseline runs on an NVIDIA RTX 6000 Ada accelerator with 18,176 CUDA cores and 48 GB of GDDR6 memory, providing

Algorithm 1 Patch-based bipolar hypervector encoding and online learning

```

1: Input: training set  $\{(\mathbf{X}^{(n)}, y^{(n)})\}$ , test set  $\{\mathbf{X}^{(m)}\}$ , dimension  $D$ , patch size  $M$ , stride  $r$ , levels  $L$ , quantization scale  $s$ , zero-point  $z$ , learning rate  $\eta$ 
2: Initialize hypervector banks  $\mathbf{B}_{i,j}$  and  $\mathbf{L}_\ell$ 
3: Initialize class hypervectors  $\mathbf{C}_c \leftarrow \mathbf{0}$  for all  $c$ 
4: // image encoding
5: function ENCODEIMAGE( $\mathbf{X}$ )
6: Quantize pixels:  $\ell_{i,j} \leftarrow \text{clip}(\lfloor X_{i,j}/s + z \rfloor, 0, L - 1)$ 
7:  $\mathbf{p}_{i,j} \leftarrow \mathbf{B}_{i,j} \odot \mathbf{L}_{\ell_{i,j}}$ 
8: for each patch  $t$  with pixels  $\mathcal{P}_t$  do
9:    $\tilde{\mathbf{h}}_t \leftarrow \sum_{(i,j) \in \mathcal{P}_t} \mathbf{p}_{i,j}$ 
10:   $\mathbf{h}_t \leftarrow \pi^t(\tilde{\mathbf{h}}_t)$ 
11: end for
12:  $\tilde{\mathbf{H}} \leftarrow \sum_t \mathbf{h}_t$ 
13:  $\mathbf{H} \leftarrow \text{sign}(\tilde{\mathbf{H}})$   $\triangleright$  bipolar binarization
14: return  $\mathbf{H}$ 
15: end function
16: // online learning (retraining over misclassified samples)
17: for each  $(\mathbf{X}^{(n)}, y^{(n)})$  in training set do
18:    $\mathbf{H} \leftarrow \text{ENCODEIMAGE}(\mathbf{X}^{(n)})$ 
19:   Compute cosine similarities:  $s_c \leftarrow \mathbf{H}^\top \mathbf{C}_c / D$  for all  $c$ 
20:   Predicted label:  $\hat{y} \leftarrow \arg \max_c s_c$ 
21:   if  $\hat{y} \neq y^{(n)}$  then
22:      $\sigma_{y^{(n)}} \leftarrow (s_{y^{(n)}} + 1)/2$ 
23:      $\sigma_{\hat{y}} \leftarrow (s_{\hat{y}} + 1)/2$ 
24:      $\mathbf{C}_{y^{(n)}} \leftarrow \mathbf{C}_{y^{(n)}} + \eta(1 - \sigma_{y^{(n)}})\mathbf{H}$ 
25:      $\mathbf{C}_{\hat{y}} \leftarrow \mathbf{C}_{\hat{y}} - \eta(1 - \sigma_{\hat{y}})\mathbf{H}$ 
26:   end if
27: end for
28: // final binarization
29:  $\mathbf{C}_c \leftarrow \text{sign}(\mathbf{C}_c)$  for all  $c$ 
30: // inference
31: for each test image  $\mathbf{X}^{(m)}$  do
32:    $\mathbf{H} \leftarrow \text{ENCODEIMAGE}(\mathbf{X}^{(m)})$ 
33:    $\hat{y}^{(m)} \leftarrow \arg \max_c \mathbf{H}^\top \mathbf{C}_c$ 
34: end for

```

up to 960 GB/s of peak memory bandwidth. For FPGA-based acceleration, we implement our HDC architecture on an AMD Alveo U280 data-center FPGA card equipped with 9024 DSP slices, on-board HBM2 memory (460 GB/s aggregate bandwidth), and a high-speed PCIe host interface.

FPGA Implementation. The proposed accelerator (Section IV) is implemented in C/C++ using AMD Vitis High-Level Synthesis (HLS) and integrated using the AMD Vitis Unified IDE v2024.2 toolchain. We target a core clock frequency of 250 MHz on the U280 and fix the hypervector-parallelism and patch-parallelism parameters to $P_D = 256$ and $P_{\text{patch}} = 16$, respectively. These choices provide a practical balance between exploiting parallelism along the hypervector dimension and across image patches, while remaining within the DSP, BRAM, and HBM bandwidth constraints of the

TABLE III
MNIST CLASSIFICATION ACCURACY COMPARISON WITH STANDARD HDC BASELINES.

Method	Accuracy (%)	Dimension
SearchHD [29]	84.43	10,000
FL-HDC [30]	88.00	10,000
TD-HDC [31]	88.92	5,000
QuantHD [28]	89.28	10,000
LeHDC [33]	94.74	10,000
LaplaceHDC [32]	94.59	10,000
Ours	95.67	10,000

TABLE IV
FASHION-MNIST ACCURACY COMPARISON.

Method	Accuracy (%)	Dimension
LaplaceHDC [32]	83.51	10,000
Ours	85.14	10,000

device.

Software Stack. We implement the patch-based HDC algorithm and online hypervector learning pipeline in Python using PyTorch for both CPU and GPU execution. CPU baselines are run with the number of worker threads set equal to the available physical cores on the EPYC server, while GPU baselines leverage CUDA and vendor-optimized libraries (cuBLAS/cuDNN) through PyTorch’s default backend. The same PyTorch implementation is used to report accuracy on MNIST and Fashion-MNIST and to profile end-to-end latency and throughput on the CPU and GPU platforms.

C. Hypervector Encoding Parameters

All experiments use a hypervector dimension of $D = 10,000$ and 256 quantization levels. We adopt non-overlapping 3×3 patches with stride 3 on 32×32 MNIST and Fashion-MNIST inputs, resulting in $K_H = K_W = 10$ and a total of 100 patches per image.

D. Accuracy Evaluation

MNIST. Our patch-based HDC encoder achieves an accuracy of **95.67%** on MNIST using a 10,000-dimensional image hypervector. This surpasses prior HDC baselines—including SearchHD [29], FL-HDC [30], TD-HDC [31], and QuantHD [28], which report accuracies in the 84–89% range—and also exceeds more advanced binary or quantized architectures such as LeHDC [33] and LaplaceHDC [32], both around 94.6–94.7%. These results show that a simple patch-aware HDC encoder can rival or surpass approaches that rely on heavy learning procedures [16] or computationally intensive manifold-based representations [18].

Fashion-MNIST. On Fashion-MNIST, our encoder achieves **85.14%** accuracy using 10,000-dimensional hypervectors, exceeding the reported 83.51% of LaplaceHDC [32]. This demonstrates that a lightweight, patch-based HDC encoder can remain competitive on more challenging visual datasets without relying on additional optimization stages.

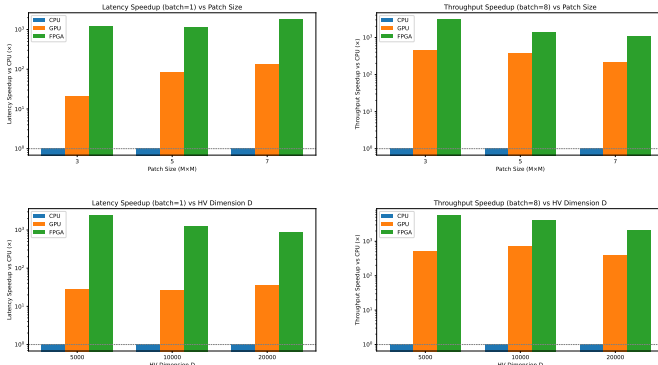


Fig. 3. Latency and throughput speedup relative to the CPU baseline. (Top) Effects of patch size using $D=10,000$. (Bottom) Scaling with hypervector dimension D . CPU speedup baseline is $1\times$.

E. Latency and Throughput Evaluation

To assess end-to-end inference performance, we compare our FPGA accelerator against optimized CPU (PyTorch, multi-threaded) and GPU (PyTorch CUDA) baselines. Latency corresponds to single-image inference (batch size 1), and throughput is measured as images per second (batch size 8 for CPU/GPU). For FPGA, throughput is simply the inverse of single-image latency, as the accelerator processes one image at a time.

Results. Figure 3 summarizes the performance. FPGA achieves sub-millisecond inference across all tested configurations (Table V), consistently outperforming both CPU and GPU. CPU exhibits high latency due to sequential patch accumulation and repeated memory transfers, while GPU benefits from tensor-level parallelism but still incurs kernel-launch overheads and limited utilization at small batch sizes. FPGA maintains a fixed, deeply pipelined datapath that exploits parallelism along both the patch and hypervector dimensions, yielding 50–60 \times lower latency than GPU and over 1000 \times lower latency than CPU. This improvement arises from mapping the entire HDC end-to-end workflow—patch encoding, global accumulation, and similarity search—onto a custom streaming dataflow architecture with dedicated compute engines and no software-level overheads.

Despite GPUs typically benefiting from larger batch sizes, FPGA achieves higher throughput even when GPU operates with batch size $B=8$. This behavior reflects the ability of a deeply pipelined streaming accelerator to sustain near-constant throughput once the pipeline is filled, whereas GPU throughput at small batches is constrained by launch latency, synchronization, and underutilization of its wide SIMD fabric. These characteristics make FPGA particularly attractive for real-time, latency-critical HDC-based image classification workloads. The results in Table V show FPGA providing approximately 1300 \times lower latency than CPU and up to 60 \times lower latency than GPU.

F. Accuracy Ablations

We evaluate the impact of patch size and hypervector dimension on MNIST classification accuracy. Figure 4 shows

TABLE V
END-TO-END MNIST INFERENCE LATENCY (BATCH SIZE = 1).

Platform	Latency (ms)	Throughput (im/s)
CPU	118.0	8.5
GPU	4.4	1906
FPGA	0.09	11,141

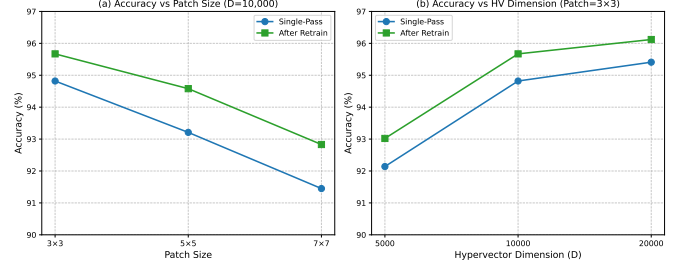


Fig. 4. Effect of patch size and hypervector dimension on MNIST accuracy. Results are shown for both single-pass training and OnlineHD-style retraining. Smaller patches preserve discriminative structure, and accuracy improves with larger D but saturates beyond 10,000.

that smaller patches consistently yield higher accuracy: 3×3 patches achieve 95.67%, outperforming 5×5 and 7×7 by 1–3%. This trend is expected, as MNIST digits contain fine-grained strokes that are best captured with high spatial resolution. Increasing the hypervector dimension D also improves accuracy, but with diminishing returns: accuracy rises from 93.02% (for $D = 5,000$) to 95.67% ($D = 10,000$), and only marginally to 96.12% at $D = 20,000$. Notably, $D=10,000$ offers the best trade-off between accuracy and computational cost, which is particularly important for FPGA deployment.

Retraining via OnlineHD’s similarity-guided updates consistently improves accuracy by 0.8–1.4% across all configurations, confirming that even a small number of refinement epochs significantly sharpens class hypervectors. Overall, these ablations validate that the chosen configuration (3×3 patches, $D=10,000$) provides the best balance of accuracy, efficiency, and hardware friendliness.

VI. CONCLUSION

We presented a spatially aware, patch-based HDC encoder and a primitive-driven FPGA accelerator for real-time image classification. By co-designing the algorithm and architecture around HDC’s binding, bundling, and permutation primitives, our approach achieves competitive accuracy while delivering orders-of-magnitude lower latency than CPU and GPU baselines.

REFERENCES

- [1] P. Kanerva, “Hyperdimensional computing: An introduction to computing in distributed representation with high-dimensional random vectors,” *Cognitive computation*, vol. 1, pp. 139–159, 2009.
- [2] D. Kleyko, D. A. Rachkovskij, E. Osipov, and A. Rahimi, “A survey on hyperdimensional computing aka vector symbolic architectures, part i: Models and data transformations,” *ACM Computing Surveys*, vol. 55, no. 6, pp. 1–40, 2022.

[3] D. Kleyko, D. Rachkovskij, E. Osipov, and A. Rahimi, "A survey on hyperdimensional computing aka vector symbolic architectures, part ii: Applications, cognitive models, and challenges," *ACM Computing Surveys*, vol. 55, no. 9, pp. 1–52, 2023.

[4] M. Hedges, I. Nunes, T. Givargis, A. Nicolau, and A. Veidenbaum, "Hyperdimensional computing: a framework for stochastic computation and symbolic ai," *Journal of Big Data*, vol. 11, no. 1, p. 145, 2024.

[5] C.-Y. Chang, Y.-C. Chuang, C.-T. Huang, and A.-Y. Wu, "Recent progress and development of hyperdimensional computing (hdc) for edge intelligence," *IEEE Journal on Emerging and Selected Topics in Circuits and Systems*, vol. 13, no. 1, pp. 119–136, 2023.

[6] A. Rahimi, P. Kanerva, L. Benini, and J. M. Rabaey, "Efficient biosignal processing using hyperdimensional computing: Network templates for combined learning and classification of exg signals," *Proceedings of the IEEE*, vol. 107, no. 1, pp. 123–143, 2018.

[7] A. Rahimi, P. Kanerva, and J. M. Rabaey, "A robust and energy-efficient classifier using brain-inspired hyperdimensional computing," in *Proceedings of the 2016 international symposium on low power electronics and design*, 2016, pp. 64–69.

[8] M. Imani, D. Kong, A. Rahimi, and T. Rosing, "Voicehd: Hyperdimensional computing for efficient speech recognition," in *2017 IEEE International Conference on Rebooting Computing (ICRC)*, 2017, pp. 1–8.

[9] M. Imani, T. Nassar, A. Rahimi, and T. Rosing, "Hdna: Energy-efficient dna sequencing using hyperdimensional computing," in *2018 IEEE EMBS International Conference on Biomedical & Health Informatics (BHI)*. IEEE, 2018, pp. 271–274.

[10] M. Imani, C. Huang, D. Kong, and T. Rosing, "Hierarchical hyperdimensional computing for energy efficient classification," in *Proceedings of the 55th Annual Design Automation Conference*, 2018, pp. 1–6.

[11] S. Datta, R. A. Antonio, A. R. Ison, and J. M. Rabaey, "A programmable hyper-dimensional processor architecture for human-centric iot," *IEEE Journal on Emerging and Selected Topics in Circuits and Systems*, vol. 9, no. 3, pp. 439–452, 2019.

[12] T. Basaklar, Y. Tuncel, S. Y. Narayana, S. Gumussoy, and U. Y. Ogras, "Hypervector design for efficient hyperdimensional computing on edge devices," *arXiv preprint arXiv:2103.06709*, 2021.

[13] L. Smets, W. Van Leekwijck, I. J. Tsang, and S. Latré, "An encoding framework for binarized images using hyperdimensional computing," *Frontiers in big data*, vol. 7, p. 1371518, 2024.

[14] P. Yi and S. Achour, "Hardware-aware static optimization of hyperdimensional computations," *Proceedings of the ACM on Programming Languages*, vol. 7, no. OOPSLA2, pp. 1–30, 2023.

[15] B. Khaleghi, H. Xu, J. Morris, and T. Š. Rosing, "tiny-hd: Ultra-efficient hyperdimensional computing engine for iot applications," in *2021 Design, Automation & Test in Europe Conference & Exhibition (DATE)*. IEEE, 2021, pp. 408–413.

[16] J. Kim, H. Lee, M. Imani, and Y. Kim, "Advancing hyperdimensional computing based on trainable encoding and adaptive training for efficient and accurate learning," *ACM Transactions on Design Automation of Electronic Systems*, vol. 29, no. 5, pp. 1–25, 2024.

[17] ———, "Efficient hyperdimensional learning with trainable, quantizable, and holistic data representation," in *2023 Design, Automation & Test in Europe Conference & Exhibition (DATE)*. IEEE, 2023, pp. 1–6.

[18] Z. Zou, Y. Kim, M. H. Najafi, and M. Imani, "Manihd: Efficient hyperdimensional learning using manifold trainable encoder," in *2021 Design, Automation & Test in Europe Conference & Exhibition (DATE)*. IEEE, 2021, pp. 850–855.

[19] Y. Ni, Y. Kim, T. Rosing, and M. Imani, "Algorithm-hardware co-design for efficient brain-inspired hyperdimensional learning on edge," in *2022 Design, Automation & Test in Europe Conference & Exhibition (DATE)*. IEEE, 2022, pp. 292–297.

[20] D. Liang, J. Shiomii, N. Miura, and H. Awano, "Distrihd: a memory efficient distributed binary hyperdimensional computing architecture for image classification," in *2022 27th Asia and South Pacific Design Automation Conference (ASP-DAC)*. IEEE, 2022, pp. 43–49.

[21] P. Neubert and S. Schubert, "Hyperdimensional computing as a framework for systematic aggregation of image descriptors," in *Proceedings of the IEEE/CVF conference on computer vision and pattern recognition*, 2021, pp. 16938–16947.

[22] F. Asgarinejad, J. Morris, T. Rosing, and B. Aksanli, "Visionhd: Towards efficient and privacy-preserved hyperdimensional computing for image data," in *Proceedings of the 29th ACM/IEEE International Symposium on Low Power Electronics and Design*, ser. ISLPED '24. New York, NY, USA: Association for Computing Machinery, 2024, p. 1–6. [Online]. Available: <https://doi.org/10.1145/3665314.3670852>

[23] R. Arbore, X. Routh, A. R. Noor, A. Kothari, H. Yang, W. Xu, S. Ping, V. Adve, T. Rosing, and M. Zhou, "Hpvmd-hdc: A heterogeneous programming system for accelerating hyperdimensional computing," *arXiv preprint arXiv:2410.15179*, 2024.

[24] W. A. Simon, U. Pale, T. Teijeiro, and D. Atienza, "Hdtorch: Accelerating hyperdimensional computing with gp-gpus for design space exploration," in *Proceedings of the 41st IEEE/ACM International Conference on Computer-Aided Design*, ser. ICCAD '22. ACM, Oct. 2022, p. 1–8. [Online]. Available: <http://dx.doi.org/10.1145/3508352.3549475>

[25] J. Kang, B. Khaleghi, T. Rosing, and Y. Kim, "Openhd: A gpu-powered framework for hyperdimensional computing," *IEEE Transactions on Computers*, vol. 71, no. 11, pp. 2753–2765, 2022.

[26] M. Imani, Z. Zou, S. Bosch, S. A. Rao, S. Salamat, V. Kumar, Y. Kim, and T. Rosing, "Revisiting hyperdimensional learning for fpga and low-power architectures," in *2021 IEEE International Symposium on High-Performance Computer Architecture (HPCA)*. IEEE, 2021, pp. 221–234.

[27] A. Dutta, S. Gupta, B. Khaleghi, R. Chandrasekaran, W. Xu, and T. Rosing, "Hdnn-pim: Efficient in memory design of hyperdimensional computing with feature extraction," in *Proceedings of the Great Lakes Symposium on VLSI 2022*, 2022, pp. 281–286.

[28] M. Imani, S. Bosch, S. Datta, S. Ramakrishna, S. Salamat, J. M. Rabaey, and T. Rosing, "Quanhd: A quantization framework for hyperdimensional computing," *IEEE Transactions on Computer-Aided Design of Integrated Circuits and Systems*, vol. 39, no. 10, pp. 2268–2278, 2019.

[29] M. Imani, X. Yin, J. Messerly, S. Gupta, M. Niemier, X. S. Hu, and T. Rosing, "Searchd: A memory-centric hyperdimensional computing with stochastic training," *IEEE Transactions on Computer-Aided Design of Integrated Circuits and Systems*, vol. 39, no. 10, pp. 2422–2433, 2019.

[30] C.-Y. Hsieh, Y.-C. Chuang, and A.-Y. A. Wu, "Fl-hdc: Hyperdimensional computing design for the application of federated learning," in *2021 IEEE 3rd International Conference on Artificial Intelligence Circuits and Systems (AICAS)*. IEEE, 2021, pp. 1–5.

[31] Y.-C. Chuang, C.-Y. Chang, and A.-Y. A. Wu, "Dynamic hyperdimensional computing for improving accuracy-energy efficiency trade-offs," in *2020 IEEE Workshop on Signal Processing Systems (SiPS)*. IEEE, 2020, pp. 1–5.

[32] S. Pourmand, W. D. Whiting, A. Aghasi, and N. F. Marshall, "Laplace-hdc: Understanding the geometry of binary hyperdimensional computing," *Journal of Artificial Intelligence Research*, vol. 82, pp. 1293–1323, 2025.

[33] S. Duan, Y. Liu, S. Ren, and X. Xu, "Lehd: Learning-based hyperdimensional computing classifier," in *Proceedings of the 59th ACM/IEEE Design Automation Conference*, 2022, pp. 1111–1116.

[34] A. Hernández-Cano, N. Matsumoto, E. Ping, and M. Imani, "Onlinehd: Robust, efficient, and single-pass online learning using hyperdimensional system," in *2021 Design, Automation & Test in Europe Conference & Exhibition (DATE)*, 2021, pp. 56–61.

[35] L. Deng, "The mnist database of handwritten digit images for machine learning research [best of the web]," *IEEE Signal Processing Magazine*, vol. 29, no. 6, pp. 141–142, 2012.

[36] H. Xiao, K. Rasul, and R. Vollgraf, "Fashion-mnist: a novel image dataset for benchmarking machine learning algorithms," *arXiv preprint arXiv:1708.07747*, 2017.